

Flow Sensitivity of CPMG Sequences with Variable Flip Refocusing and Implications for CSF Signal Uniformity in 3D-FSE Imaging

R. F. Busse¹

¹Global Applied Science Lab, GE Healthcare, Madison, WI, United States

RARE (FSE, TSE) with variable flip refocusing enables acquisition of 3D T2-weighted image sets of the brain with high resolution in all dimensions within ~5 minutes (1). Even with echo trains lasting >500ms, low flips at the beginning of the train slow relaxation and thus reduce “equivalent” echo times (2) to clinically appropriate values. Increasing flips, calculated to target specific signal levels throughout the train (3), further counteracts T2-decay to mitigate blurring. While soft tissue CNR may be excellent, however, CSF may appear dark in certain areas where flow may be considerable. The goal of this work was to explore the sensitivity of variable flip refocusing to flow. It is hypothesized that as refocusing flip angles decreased and/or net gradient area between refocusing RF pulses increased, the sensitivity to flow would increase.

Methods

The Extended Phase Graph (EPG) algorithm enables calculation of signal contribution from numerous spin and stimulated echo pathways (4). Transverse magnetization accrues phase during each interval between RF pulses. The phase accrued is a function of the net gradient area, A_G , and position, x , during interval n :

$$\phi_n = \gamma(\vec{x}_n \cdot \vec{A}_G)$$

Net gradient area is controllable and is directly related to the total distance in k-space traveled ($2k_{x,max}$) and inversely to spatial resolution (p_x , the pixel dimension in the frequency encode dimension). If the phase encode gradients are rewound and the net gradient area is due entirely to the frequency encode gradient, then

$$2k_{x,max} = \frac{1}{p_x} = \frac{\gamma}{2\pi} A_G \quad \text{therefore} \quad A_G = \frac{2\pi/\gamma}{p_x}$$

Alternatively, additional “crusher” gradients may be added to further dephase FID signals generated by the refocusing RF pulses, a source of artifact.

For static material, x_n is constant, thus the phase accrued between RF pulses is always the same and readily refocused. For constant velocity motion/flow, however, an additional phase term that increases with each successive echo exists, proportional to the gradient area, velocity, and echo spacing:

$$\phi_n = \gamma(\vec{x}_0 \cdot \vec{A}_G) + \gamma(\vec{v} \cdot \vec{A}_G)(n \cdot \Delta TE)$$

Pseudo-steady state (5), the spin system condition that produces maximal signal given low and variable flip refocusing, requires coherent superposition of numerous signal pathways. Motion, however, causes differing amounts of phase to accrue in different pathways. Signal loss results when signal pathways do not add constructively. This effect was modeled with an EPG algorithm modified to incorporate phase accrual due to motion, programmed for analysis using MATLAB (Mathworks).

To assess the sensitivity of variable flip CPMG to motion, several refocusing flip angle schedules were designed with a variety of minimum flip angles such as shown in Fig. 1a. Velocities between 0 and 4 cm/s in the x-direction were considered, consistent with observed CSF flow velocities (6). Echo spacing of 4ms and $A_G = (2\pi/\gamma) / p_x$ were used, where $p_x = 1\text{mm}$.

Volunteer experiments using a 3D-FRFSE sequence were performed (GE Signa 3T) to assess the effect of refocusing flip angle schedule and net gradient area on signal intensity in CSF. Variable flip refocusing schedules with minimum angles of 20°, 40°, and 60° were used. Net gradient area was either the minimum for $p_x = 1\text{mm}$ in-plane resolution, or increased to 1.5x this for extra FID spoiling. Each whole-brain image set with 1.4mm slice resolution was acquired in 5 minutes.

Results

Figure 1 shows the results of the numerical modeling experiment given flip schedules shown in 1a. Signal at each echo in the pulse train is shown in Fig. 1b, with solid lines representing static fluid and dashed lines representing fluid flowing at 1 cm/sec. Lower refocusing flip angles resulted in signal loss for the flowing material. Total signal (sum of signal over the entire pulse train, normalized to total signal in a static material) is shown as a function of flow velocity in Fig 1c. Lower refocusing flip angles resulted in a lower “cutoff” velocity after which signal loss was observed.

Figure 2 shows midline sagittal views from the volunteer experiment data sets. Little or no loss of signal was observed when the minimum flip angle was 60° and net gradient area was minimized. However, as the minimum flip angle was decreased, signal loss was observed in areas of high flow (arrows). Likewise, when the additional crusher gradient area was applied, observed signal loss was more prevalent in high flow regions.

Discussion

FSE with variable flip refocusing is a means to acquire large volumetric datasets with T2-weighting in a relatively short time, but it is considerably more sensitive to motion and flow than conventional 180° refocusing. Limiting the minimum refocusing flip angle can mitigate signal loss, but this reduces the usable length of the readout train, and thus the acquisition efficiency. Limiting the net gradient area can also reduce signal loss, but may allow artifacts due to unspoiled FID signal to contaminate the images.

Given that CSF flow is known to oscillate cyclically with the heart cycle (5), it may be possible to gate the acquisition in order to synchronize the portion of the readout train with lowest flip angles to the time of slowest flow. It may also be possible to align extra crusher gradients to be perpendicular to flow, but this may increase echo spacing. Understanding the unique motion sensitivity of variable flip FSE can be used to tailor the pulse sequence to reduce troublesome signal voids. Such understanding may also be used to additional advantage, for instance as a means of visualizing flow or purposefully eliminating signal from flowing blood.

References: (1) Mugler, Proc ISMRM 2000, p687; (2) Busse, Proc ISMRM 2005, p2344; (3) Hennig, MRM 51:68 (2003); (4) Hennig, Concepts in MR 3:125 (1991); (5) Alsop, MRM 37:176 (1997); (6) Bhadelia, AJNR:16 (1995)

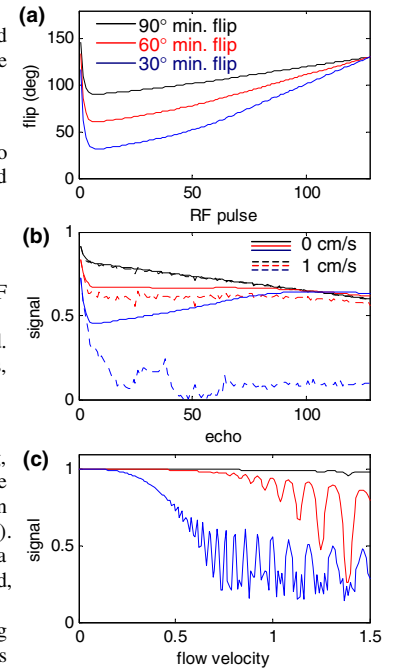


Figure 1: Numerical Model

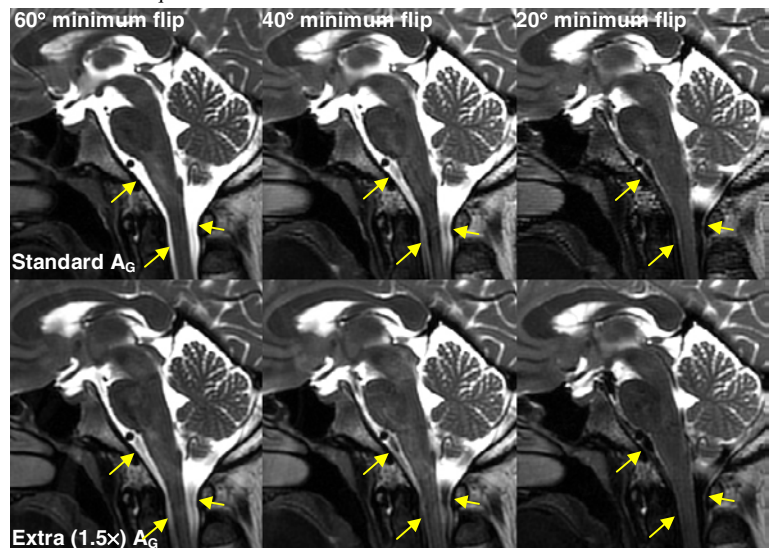


Figure 2: Volunteer 3D-FRFSE Imaging